

Use of Polyimide-*graft*-Bisphenol A Diglyceryl Acrylate as a Reactive Noncovalent Dispersant of Single-Walled Carbon Nanotubes for Reinforcement of Cyanate Ester/Epoxy Composite

Wei Yuan,[†] Junluo Feng,[†] Zaher Judeh,[†] Jie Dai,[‡] and Mary B. Chan-Park^{*,†}

[†]School of Chemical and Biomedical Engineering, Nanyang Technological University, 62 Nanyang Drive, Singapore 637459, Singapore, and [‡]DSO National Laboratories, 20 Science Park Drive, Singapore 118230, Singapore

Received June 26, 2010. Revised Manuscript Received November 9, 2010

Dispersion of single-walled carbon nanotubes (SWNTs) into individuals or small bundles and strong nanotube/matrix interfacial strength remain as challenges in exploiting the excellent mechanical properties of SWNTs in structural composites. Noncovalent functionalization of SWNTs is an attractive option for compatibilization of nanotubes with the matrix as it does not destroy the nanotube graphene structure. We have designed and successfully synthesized a new reactive comb-like polymer, polyimide-*graft*-bisphenol A diglyceryl acrylate (PI-BDA), which is shown to be highly effective in dispersing SWNTs into individual nanotubes or small bundles, as evidenced by transmission electron microscopy (TEM) and UV-vis-NIR absorption spectra. SWNTs dispersed with PI-BDA were added to a thermosetting resin blend of cyanate ester and epoxy (CE-EP) (70/30, w/w) and composite fibers with SWNT loading ranging from 0 to 1.5 wt % were successfully fabricated. The strong π - π interaction between SWNTs and PI-BDA backbone was evidenced by Raman spectra, and the covalent reaction between PI-BDA side-chain and matrix was confirmed by FT-IR and ¹H NMR. Our designed dispersant interacts noncovalently with nanotubes but reacts with the thermosetting matrix. With addition of PI-BDA dispersant, only 1 wt % SWNTs optimally increases the tensile modulus, strength, and toughness by 80% (to 4.70 ± 0.24 GPa), 70% (to 142.3 ± 6.9 MPa), and 58% (4.1 ± 0.4 MJ m⁻³) compared to the neat resin blend (with $E = 2.61 \pm 0.14$ GPa, $\sigma = 83.7 \pm 3.3$ MPa, and $T = 2.6 \pm 0.2$ MJ m⁻³). Improvement in thermal properties was also observed.

Introduction

Carbon nanotubes (CNTs) are thought to be an ideal material for reinforcement in ultrastrong lightweight polymer composites due to their low mass density, large aspect ratio (typically ca. 300–1000), and superior mechanical properties.^{1,2} Outstanding mechanical properties (specifically, tensile strength of 500–2000 MPa and modulus of 15–169 GPa) of CNT/polymer composites have recently been reported, though achieved with special nanotubes and/or nonconventional processing techniques.^{3–5} With conventional composite processing techniques and common CNTs, the properties of resultant CNT-reinforced composites, especially using common thermosetting matrices,

have generally been far inferior than theoretically predicted.^{6–9} For example, Zhu et al.⁶ reported 30% increase in Young's modulus (from 2.03 to 2.63 GPa) and 14% increase in tensile strength (from 83.2 to 95.0 MPa) for epoxy composites reinforced with 1 wt % fluorinated single-walled carbon nanotubes (SWNTs). Recently, our group reported 85% and 17% increases in tensile strength and modulus, respectively, for cyanate ester composites reinforced with 1 wt % SWNTs¹⁰ and 39% and 18%, respectively, for epoxy composites with 0.5 wt % SWNTs.¹¹ The modest improvements with CNTs are still beneficial for reinforcing thermosetting resins for adhesives or even carbon fiber reinforced hierarchical composites^{12–14} in which the small size of CNTs makes the nanotube-reinforced

*Corresponding author e-mail: mbechan@ntu.edu.sg.

- (1) Coleman, J. N.; Khan, U.; Gun'ko, Y. K. *Adv. Mater.* **2006**, *18*, 689.
- (2) Moniruzzaman, M.; Winey, K. I. *Macromolecules* **2006**, *39*, 5194.
- (3) Ma, W. J.; Liu, L. Q.; Zhang, Z.; Yang, R.; Liu, G.; Zhang, T. H.; An, X. F.; Yi, X. S.; Ren, Y.; Niu, Z. Q.; Li, J. Z.; Dong, H. B.; Zhou, W. Y.; Ajayan, P. M.; Xie, S. S. *Nano Lett.* **2009**, *9*, 2855.
- (4) Shim, B. S.; Zhu, J.; Jan, E.; Critchley, K.; Ho, S. S.; Podsiadlo, P.; Sun, K.; Kotov, N. A. *ACS Nano* **2009**, *3*, 1711.
- (5) Cheng, Q. F.; Bao, J. W.; Park, J.; Liang, Z. Y.; Zhang, C.; Wang, B. *Adv. Funct. Mater.* **2009**, *19*, 3219.
- (6) Zhu, J.; Kim, J.; Peng, H.; Margrave, J. L.; Khabashesku, V. N.; Barrera, E. V. *Nano Lett.* **2003**, *3*, 1107.
- (7) Sun, L.; Warren, G. L.; O'Reilly, J. Y.; Everett, W. N.; Lee, S. M.; Davis, D.; Lagoudas, D.; Sue, H. J. *Carbon* **2008**, *46*, 320.

- (8) Chen, Z. K.; Yang, J. P.; Ni, Q. Q.; Fu, S. Y.; Huang, Y. G. *Polymer* **2009**, *50*, 4753.
- (9) Chen, D.; Liu, T. X.; Zhou, X. P.; Tjiu, W. C.; Hou, H. Q. *J. Phys. Chem. B* **2009**, *113*, 9741.
- (10) Che, J. F.; Chan-Park, M. B. *Adv. Funct. Mater.* **2008**, *18*, 888.
- (11) Che, J.; Yuan, W.; Jiang, G.; Dai, J.; Lim, S. Y.; Chan-Park, M. B. *Chem. Mater.* **2009**, *21*, 1471.
- (12) Qian, H.; Greenhalgh, E. S.; Shaffer, M. S. P.; Bismarck, A. *J. Mater. Chem.* **2010**, *20*, 4751.
- (13) Qian, H.; Bismarck, A.; Greenhalgh, E. S.; Kalinka, G.; Shaffer, M. S. P. *Chem. Mater.* **2008**, *20*, 1862.
- (14) Bekyarova, E.; Thostenson, E. T.; Yu, A.; Kim, H.; Gao, J.; Tang, J.; Hahn, H. T.; Chou, T. W.; Itkis, M. E.; Haddon, R. C. *Langmuir* **2007**, *23*, 3970.

matrix (also called the hybrid matrix) processable like the neat resin. The mechanical properties of “hybrid matrix” are improved because CNTs have strength (10–63 GPa)^{15,16} far superior to most thermosetting matrices, and even carbon fibers (~250 MPa).¹⁷ Further, the nanoscale size of CNTs enables them to be applied as reinforcements in low-dimensional (e.g., 2-D) structures, e.g., polymer fibers, foams, and films,^{4,10,18} where other conventional microscale fillers would be too large for inclusion. CNTs can also be used to produce multifunctional structural composites with unique thermal, electrical, and optical properties.²

The general poor improvement in the mechanical properties of CNT/polymer composite can be partially attributed to the poor nanotube dispersion and nanotube/matrix stress transfer. Due to strong van der Waals forces between the nanotubes, CNTs are usually bundled which would result in intertube slippage with applied stress and poor mechanical properties of CNT composites. Further, the graphene structure of CNTs is atomically smooth and highly hydrophobic so that stress transfer to a typical polymer composite matrix, which is usually relatively polar, is poor. To exploit the high mechanical properties of nanotubes in composites, the nanotubes have to be well-dispersed and the nanotube/matrix interface has to be strong.

In most of the solution-processed composite studies, the CNTs were covalently functionalized.^{6,19,20} The SWNTs used in both our two studies^{10,11} were covalently functionalized via grafting of organic molecules and seem to be bundled. It appears that covalent functionalization^{6,10,11,19,20} can only moderately improve the mechanical properties of composites. The high density of functionalization needed for effective stress transfer disrupts the extended π conjugation in nanotubes, leading to decreased mechanical properties. Moreover, covalent functionalization is typically not effective for individually dispersing high concentration of CNTs. On the contrary, noncovalent functionalization using surfactant or polymer has been shown to be effective in individually dispersing nanotubes without compromising the nanotube graphene structure.^{21–23} Conjugated and aromatic condensation polymers, such as poly(phenylene ethynyls),²⁴ poly-

thiophene,^{25,26} polybenzimidazole,²⁷ and polyimide,^{28,29} which interact with CNTs via strong π – π interaction, have been used to disperse CNTs and reinforce polymer matrix in previous studies. The π – π interaction has been suggested to be the strongest noncovalent interaction by a recent theoretical modeling study.³⁰ However, these studies mainly focus on thermoplastic matrices and only a few studies using noncovalently functionalized CNTs to reinforce thermosetting matrices have been reported.³¹

Cyanate ester (CE) resins are high-performance structural thermosets widely used in the electronics and aerospace industries due to their outstanding adhesive, thermal, mechanical, and electrical properties.³² A drawback of CE is its brittleness resulting from the highly cross-linked structure which often restricts its structural applications. Copolymerizing CE with other thermosetting resins such as epoxy (EP) has been proven to be effective in toughening CE with enhanced processability and at low cost.³³ This thermostable, processable, and relatively tough cyanate ester/epoxy blend is a favorable matrix widely used in electronic and aerospace applications. Addition of inorganic nanofillers has been confirmed to be an effective approach for toughening thermosets without compromising their thermal properties.^{10,34}

This paper reports our design and synthesis of a reactive noncovalent polymeric dispersant for SWNTs: polyimide-graft-bisphenol A diglyceryl acrylate (PI-BDA) (Scheme 1). The polyimide backbone can strongly interact with the nanotube via noncovalent interaction, while the side chain facilitates dispersion and the hydroxyl group on the graft enables reaction with the matrix. The high efficacy of PI-BDA at dispersing SWNTs in dimethylformamide (DMF) was assessed with transmission electron microscopy (TEM) and UV–vis–NIR absorption spectra. PI-BDA was used to disperse SWNTs in a thermosetting resin blend of cyanate ester and epoxy (CE-EP) (70/30, w/w) (Scheme 2). Two series of SWNT composites, one with PI-BDA dispersed-SWNTs and one without, with nanotube content ranging from 0 to 1.5 wt % were fabricated. For convenience, SWNT/resin and SWNT/PI-BDA/resin composites are hereafter denoted as SWNTs/R and SWNTs/PI-BDA/R respectively. The nanotube dispersion and nanotube/matrix interaction were examined by field-emission scanning electron microscopy (FE-SEM), Raman spectra, FT-IR, and ¹H NMR. The tensile properties, glass transition temperature (T_g), and thermal decomposition temperature (T_d) of the cured composites were measured as a function of SWNT content.

(15) Yu, M. F.; Lourie, O.; Dyer, M. J.; Moloni, K.; Kelly, T. F.; Ruoff, R. S. *Science* **2000**, *287*, 637.

(16) Yu, M. F.; Files, B. S.; Arepalli, S.; Ruoff, R. S. *Phys. Rev. Lett.* **2000**, *84*, 5552.

(17) Lubin, G., Ed. *Handbook of Composites*; Van Nostrand Reinhold: New York, 1982; p 234.

(18) Jell, G.; Verdejo, R.; Safinia, L.; Shaffer, M. S. P.; Stevens, M. M.; Bismarck, A. *J. Mater. Chem.* **2008**, *18*, 1865.

(19) Zhou, C. J.; Wang, S. F.; Zhang, Y.; Zhuang, Q. X.; Han, Z. W. *Polymer* **2008**, *49*, 2520.

(20) Gao, J. B.; Itkis, M. E.; Yu, A. P.; Bekyarova, E.; Zhao, B.; Haddon, R. C. *J. Am. Chem. Soc.* **2005**, *127*, 3847.

(21) Richard, C.; Balavoine, F.; Schultz, P.; Ebbesen, T. W.; Mioskowski, C. *Science* **2003**, *300*, 775.

(22) Yan, L. Y.; Poon, Y. F.; Chan-Park, M. B.; Chen, Y.; Zhang, Q. *J. Phys. Chem. C* **2008**, *112*, 7579.

(23) Zou, J. H.; Liu, L. W.; Chen, H.; Khondaker, S. I.; McCullough, R. D.; Huo, Q.; Zhai, L. *Adv. Mater.* **2008**, *20*, 2055.

(24) Chen, J.; Ramasubramaniam, R.; Xue, C.; Liu, H. *Adv. Funct. Mater.* **2006**, *16*, 114.

(25) Kim, K. H.; Jo, W. H. *Macromolecules* **2007**, *40*, 3708.

(26) Kim, K. H.; Jo, W. H. *Carbon* **2009**, *47*, 1126.

(27) Okamoto, M.; Fujigaya, T.; Nakashima, N. *Adv. Funct. Mater.* **2008**, *18*, 1776.

(28) Delozier, D. M.; Watson, K. A.; Smith, J. G.; Clancy, T. C.; Connell, J. W. *Macromolecules* **2006**, *39*, 1731.

(29) Li, N. W.; Zhang, F.; Wang, J. H.; Li, S. H.; Zhang, S. B. *Polymer* **2009**, *50*, 3600.

(30) Yang, M.; Koutsos, V.; Zaiser, M. *J. Phys. Chem. B* **2005**, *109*, 10009.

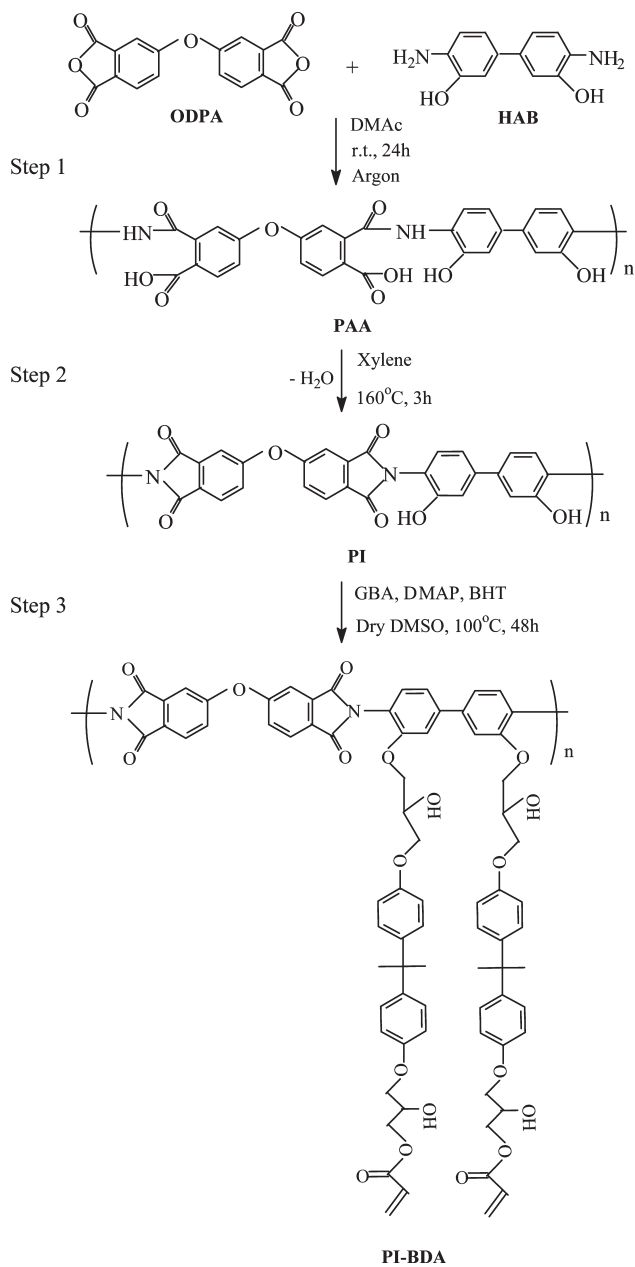
(31) Gong, X. Y.; Liu, J.; Baskaran, S.; Voise, R. D.; Young, J. S. *Chem. Mater.* **2000**, *12*, 1049.

(32) Laskoski, M.; Dominguez, D. D.; Keller, T. M. *J. Polym. Sci., Part A: Polym. Chem.* **2006**, *44*, 4559.

(33) Liang, G. Z.; Zhang, M. X. *J. Appl. Polym. Sci.* **2002**, *85*, 2377.

(34) Pan, Y.; Xu, Y.; An, L.; Lu, H.; Yang, Y.; Chen, W.; Nutt, S. *Macromolecules* **2008**, *41*, 9245.

Scheme 1. Synthesis of Hydroxyl Polyimide (PI) and Polyimide-graft-bisphenol A Diglyceryl Acrylate (PI-BDA)



Experimental Section

Materials. 3,3'-Dihydroxy-4,4'-diaminobiphenyl (HAB, 97%) was purchased from Tokyo Chemical Industry. α -Glycidyl terminated bisphenol A acrylate (GBA, Scheme 2c) with a molecular weight of 450 was supplied as Ebecryl 3605 from UCB chemicals (Malaysia). It was freeze-dried at -55°C for 2 days before use. 4,4'-Oxydiphthalic anhydride (ODPA, 97%), 4-(dimethylamino)pyridine (DMAP, 99%), butylated hydroxytoluene (BHT, 99%), sodium hydrogen carbonate (NaHCO_3 , 99.5%), *N,N'*-dimethylacetamide (DMAc), xylene, dimethyl sulfoxide (DMSO), *N,N'*-dimethylformamide (DMF), and methanol were obtained from Sigma-Aldrich. DMAc and DMSO were distilled over calcium hydride and xylene over sodium wire before use. All other chemicals were used as received. Bisphenol A cyanate ester resin (CE, Scheme 2a) was purchased from Shanghai Huifeng Technical & Business Co., Ltd. (Shanghai, China) with the trade name HF-1. Diglycidyl ether bisphenol A epoxy resin (EP, Scheme 2b),

was purchased from Wuxi Resin Factory (China) with the trade name E20.

SWNTs were purchased from Chengdu Research Institute of Organic Chemistry (China); they were produced by the chemical vapor deposition (CVD) method and have diameters of 1–2 nm, lengths of 5–30 μm , and purity of $\sim 90\%$. They were purified with thermal oxidation (350 $^\circ\text{C}$ for 2 h in air) followed by acid treatment (refluxing in 6 M HCl solution for 12 h) before use.

Synthesis of Hydroxyl Polyimide (PI). The reaction is shown in Steps 1–2 in Scheme 1. In a typical experiment, HAB (1.080 g, 5.00 mmol) was dissolved in 40 mL of freshly distilled DMAc in a round-bottom flask under argon protection. After the solution was cooled at 0°C for 15 min, ODPA (1.550 g, 5.00 mmol) was added to the solution with vigorous stirring. The mixture was then warmed to room temperature and magnetically stirred for 24 h under argon atmosphere to form poly(amic acid) (PAA) solution. Then dry xylene (40 mL) was added to this solution and stirred at 160°C for 3 h to eliminate the water formed in the imidization reaction. After cooling to room temperature, the reaction mixture was added dropwise into a large excess of methanol to precipitate the PI. The precipitate was filtered and repeatedly washed with a large amount of methanol and then with THF. The separated precipitate was dried at 80°C under vacuum for 24 h. The yield was 2.040 g (83% yield).

Synthesis of Polyimide-graft-Bisphenol A Diglyceryl Acrylate (PI-BDA). The reaction is shown in Step 3 in Scheme 1. DMAP was added as the catalyst³⁵ and BHT was added to prevent homopolymerization of acrylate double bond on the BDA side chain.³⁶ Typically, PI (0.588 g, 1.20 mmol of repeat unit) was dissolved in 40 mL of dry DMSO at 60°C in a round-bottom flask with a water condenser under argon atmosphere. After dissolution of DMAP (0.293 g, 2.40 mmol), a solution of GBA (1.188 g, 2.64 mmol) together with BHT (0.018 g, 0.08 mmol) in 20 mL of dry DMSO was added, and the resulting mixture was stirred at 100°C for 48 h. After removal of some DMSO with a rotary evaporator, the mixture was added dropwise into bulk methanol with vigorous stirring. The precipitate was filtered and washed several times with 0.2 M HCl solution, then with 5% NaHCO_3 solution, and finally with water. The side-chain grafted polyimide (PI-BDA) product was dried under vacuum at room temperature for 48 h. The yield was 0.850 g (51% yield).

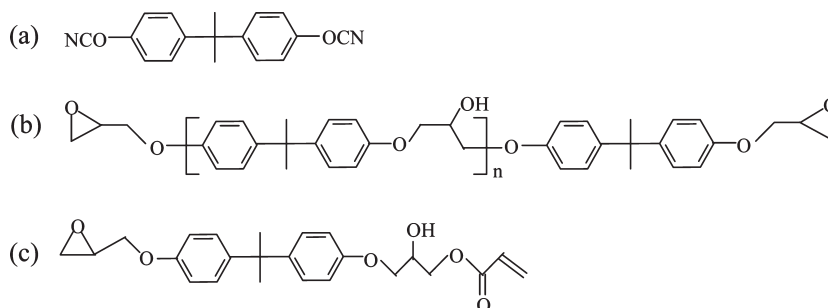
Preparation of SWNT Dispersions. To prepare SWNT/PI-BDA dispersion, 10 mg of purified SWNTs and 10 mg of PI-BDA were first added into 10 mL of DMF. Then the mixture was sonicated with a tip sonicator for 10 min followed by further sonication in a sonicator bath for 30 min. The resulting stable and homogeneous solution had a SWNT concentration of 1 mg/mL. Pristine SWNT suspension in DMF was prepared by the same procedure without the addition of PI-BDA. For Raman characterization, the SWNT/PI-BDA solution was filtered and washed thoroughly with DMF to remove any free surfactant, and the resultant powder was dried.

Evaluation of SWNT Dispersion Stability by Visual Observation. Pristine SWNTs and SWNT/PI-BDA solutions with SWNT concentration of 1 mg/mL were prepared. To clearly observe whether there are SWNT aggregates in the solution, parts of these two solutions were also diluted by 50 times to afford solutions with low nanotube concentration (0.02 mg/mL). All these solutions (before and after dilution) were left standing for different times

(35) van Dijk-Wolthuis, W. N. E.; Franssen, O.; Talsma, H.; van Steenbergen, M. J.; Kettenes-van den Bosch, J. J.; Hennink, W. E. *Macromolecules* **1995**, *28*, 6317.

(36) Bahar, Y.; Aylin Ziyilan, A.; Nihan Celebi, O.; Duygu, A. *J. Polym. Sci., Part A: Polym. Chem.* **2008**, *46*, 2290.

Scheme 2. Structures of (a) Bisphenol A Cyanate Ester (CE), (b) Diglycidyl Ether Bisphenol A Epoxy (EP), and (c) α -Glycidyl Terminated Bisphenol A Acrylate (GBA)



(immediately, 7 days, and 6 months) and the homogeneity was evaluated by visual observation.

Fabrication of Fibers. SWNT/PI-BDA solution (1 mg SWNTs/mL) was first prepared via the method described above. CE-EP matrix was prepared by mixing CE (70 wt %) and EP (30 wt %) at 110 °C for 30 min. A 2-g portion of CE-EP matrix was added to measured quantities of SWNT/PI-BDA dispersion to produce solutions of SWNTs/PI-BDA/R with different SWNT loadings. After sonication in a sonicator bath for 10 min, the solution was cast onto glass substrates, which were placed on a hot plate at about 50 °C for 1 h to slowly remove most of the DMF. The glass substrates were then transferred to a vacuum oven and dried under vacuum at 90 °C for 1 h and 100 °C for 2 h. Subsequently, the blend was collected from the glass substrates and the bubbles were removed using a vacuum oven. The blend was then used to fabricate SWNT/PI-BDA/R composite fibers using our custom-made reactive spinning device.^{10,11} After spinning, the fibers were pre-cured for 6 h under a UV lamp (intensity of 30 mW/cm², with on/off cycle of 15 min/15 min) which was filtered with a dish of water, and then further thermal cured at 100 °C/1 d under vacuum followed by 120 °C/2 h, 150 °C/2 h, 180 °C/2 h, and postcuring of 200 °C/4 h at atmospheric pressure. Neat CE-EP fibers and pristine SWNTs-reinforced fibers (SWNTs/R) were also prepared by similar method. Details of fiber fabrication can be found in the Supporting Information Part 1.

Verifying the Reaction between PI-BDA and CE. To verify, with FT-IR, the addition reaction between -OH on PI-BDA with the CE, PI-BDA/CE blend (30/70, w/w) was first dissolved in DMF, then several drops were cast onto a potassium bromide (KBr) pellet. The DMF was removed under vacuum at 80 °C for 2 h. Then the sample was characterized by FT-IR before and after heating at 120 °C for 1 h. To verify the reaction using ¹H NMR, PI-BDA/CE blend (30/70, w/w) was dissolved in deuterated dimethylsulfoxide (DMSO-*d*₆), and ¹H NMR spectra of the sample were collected before and after heating at 120 °C for 1 h.

Characterization. ¹H NMR spectra of PI, PI-BDA, and PI-BDA/CE (30/70, w/w) blend were recorded on a Bruker (300 MHz) NMR instrument using DMSO-*d*₆ as solvent. Fourier transform infrared (FT-IR) spectra of PI-BDA/CE (30/70, w/w) blend before and after heating at 120 °C for 1 h were recorded on a Nicolet 5700 FT-IR instrument. The molecular weight of PAA and PI-BDA was analyzed by gel permeation chromatography (GPC) carried out on a Shimadzu LC-20A Series GPC system equipped with a pump, BC-PL gel mixed columns, and a refractive index detector (RID-10A). DMF with 0.02 M LiBr was used as the eluting solvent and polystyrene standards were used as the reference. Thermogravimetric analysis (TGA) of neat CE-EP and its composites was performed on a Netzsch STA 409 PG/PC instrument under a nitrogen atmosphere, with a heating rate of 10 °C/min from 50 to 800 °C. Glass-transition

temperatures (*T*_g) of neat CE-EP and its composites were determined from differential scanning calorimetry (DSC) performed on a Mettler Toledo DSC 822e instrument under N₂ at a heating/cooling rate of 20 °C/min from 50 to 230 °C. The *T*_g was calculated from the midpoint of the change in slope on the second heating run. Raman spectra were obtained with a Renishaw in Via Raman microscope with HeNe laser excitation wavelength of 633 nm. UV-vis-NIR absorption spectra of the nanotube solutions were recorded on a Varian Cary 5000 UV-vis-NIR spectrophotometer. Optical microscopy characterization of SWNT-(0.2 wt %)/R and SWNT(0.2 wt %)/PI-BDA/R composites was carried out on an Olympus SZX12 microscope at a magnification of 144×. Transmission electron microscopy (TEM) measurements were carried out on a JEOL 2100F high-resolution scanning electron microscope operating at 200 kV. Pristine or PI-BDA functionalized SWNTs dispersed in DMF was diluted and drop cast onto a carbon-coated copper grid followed by solvent evaporation. The dispersion of SWNTs in composite fibers was examined with a JEOL JSM-6700F field-emission scanning electron microscope (FE-SEM). Uncured SWNT(1 wt %)/R and SWNT(1 wt %)/PI-BDA/R spun fibers were redispersed in DMF with only mild shaking followed by filtration through a 0.2- μ m Al₂O₃ membrane and washing several times with large quantity of DMF to remove any free polymer. These samples were coated with gold and examined with FE-SEM. The fracture surfaces of composites after tensile testing were also coated with gold for FE-SEM observation. Tensile properties of neat CE-EP and composite fibers were determined using an Instron model 5543 mechanical tester at room temperature. The gauge length was 25 mm and the diameter was estimated by optical microscopy. A 10 N load cell and a cross head speed of 2.54 mm/min were used to do the testing. At least 10 samples were tested and the results were averaged.

Results and Discussion

Synthesis and Characterization of PI and PI-BDA. The structures of the synthesized PI and PI-BDA were confirmed by ¹H NMR spectroscopy. The complete assignment of the proton signals is shown in Figure 1. In the ¹H NMR spectrum of PI (Figure 1A), characteristic peaks of the phenolic OH and aromatic protons are shown at δ 10.1 (a) and 7.1–8.2 (b–g) ppm, respectively. In the ¹H NMR spectrum of PI-BDA (Figure 1B), the phenolic OH signals completely disappeared while the aromatic protons of the PI backbone appeared at δ 7.0–8.2 ppm (b–g). New peaks at δ 6.7 ppm (k) and δ 7.0 ppm (l) are attributed to the aromatic protons of the grafted BDA side chain. The peaks at δ 5.8 (s, CH₂), 6.1 (q, CH), 6.2 ppm

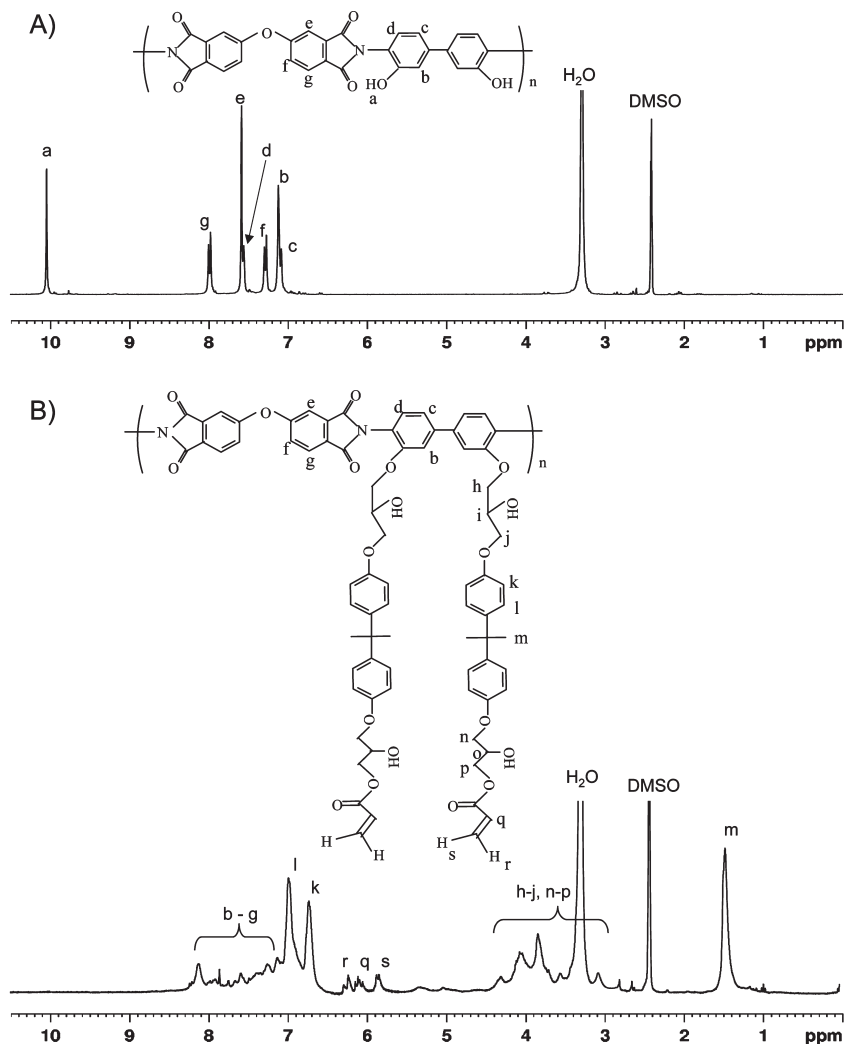


Figure 1. ^1H NMR spectra of (A) PI and (B) PI-BDA.

(r, CH_2) are attributed to the $-\text{OCOCH}=\text{CH}_2$ terminal group. The peak at δ 1.5 ppm (m) is attributed to $-\text{CH}_3$ groups, while the peaks at δ 3.0–4.5 ppm are assigned to the aliphatic protons of $-\text{OCH}$ (i and o) and $-\text{OCH}_2$ (h, j, n and p) in BDA side chain. The complete disappearance of the peak at δ 10.1 ppm (a) and the appearance of new resonance peaks (h–s) confirm that BDA is 100% grafted on every pendant $-\text{OH}$ of PI-BDA. The molecular weights (M_n) of poly(amic acid) (PAA) and PI-BDA were measured by GPC. Compared to PAA ($M_n = 2.7 \times 10^4$ g/mol), PI-BDA has expectedly higher molecular weight ($M_n = 3.9 \times 10^4$ g/mol). The polydispersity indices of PAA and PI-BDA were 1.38 and 1.35, respectively.

Solubility of PI-BDA Functionalized SWNTs. The dispersion stability of SWNT solutions prepared in DMF with and without PI-BDA was evaluated by visual observation at different standing times after sonication (Figure 2). Immediately after sonication, high SWNT concentration solutions (1 mg/mL) of both pristine SWNTs and SWNTs/PI-BDA are black (Figure 2A vials a and c), and we cannot tell whether there are nanotube aggregates in these solutions due to the darkness. After dilution to 0.02 mg/mL, suspended nanotube aggregates can be clearly seen in pristine SWNT solution (Figure 2A, vial b), whereas the

diluted SWNT/PI-BDA solution appears free from SWNT aggregates (Figure 2A, vial d). After 7 days, pristine SWNTs completely settled at the bottom of the vials (Figure 2B, vials a and b). The SWNT/PI-BDA solutions were very stable and did not precipitate after 7 days (Figure 2B, vials c and d), or even after six months of standing at room temperature. These phenomena indicate that PI-BDA significantly improves the solubility of SWNTs in DMF and provides long-term dispersion stability.

The dispersion of pristine SWNTs and PI-BDA functionalized SWNTs in DMF was also examined by TEM (Figure 3). As shown in Figure 3A1 and A2, pristine SWNTs are highly entangled with each other and the bundle size (about 30 nm or larger) is not uniform. Figure 3A3 reveals that the SWNT surface is very clean. After functionalization with PI-BDA, the bundle size becomes much smaller (Figure 3B1), and most of the SWNTs appear to be dispersed as individual tubes or very small bundles (Figure 3B2). A higher resolution TEM image (Figure 3B3) reveals clearly that the SWNTs are covered with a layer of coating, which is believed to be PI-BDA wrapped on the SWNT surface. It should be noted that the thickness of the PI-BDA layer is not uniform. A lower magnification TEM image (Supporting Information, Figure S5) shows that the SWNT length

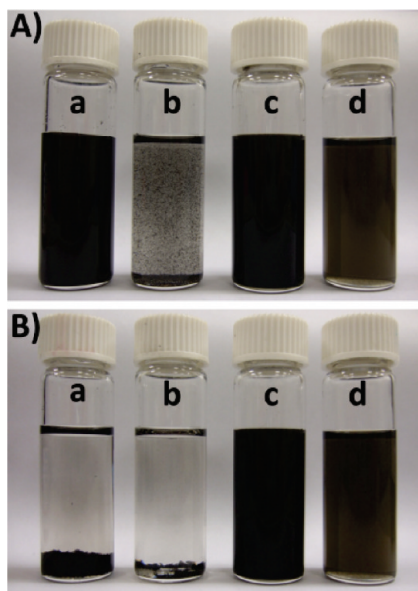


Figure 2. Visual observation of (a and b) pristine SWNT and (c and d) SWNTs/PI-BDA in DMF at different standing times after sonication: (A) immediately; (B) 7 days. The SWNT concentration of a and c is 1 mg/mL and of b and d is 0.02 mg/mL.

(at least 1–2 μm) is not significantly reduced after non-covalent functionalization with PI-BDA, which is different from the observation of chopped CNTs (length usually less than 1 μm) after covalent modification.^{37,38} The high efficacy of PI-BDA at dispersing SWNTs into individual nanotubes or small bundles was also verified by UV–vis–NIR (Supporting Information, Figure S6). We postulate that the high efficiency of PI-BDA at dispersing SWNTs is attributed to its comb-like structure, where the PI backbone has strong π – π interaction with SWNTs wall and the BDA graft imparts strong repulsive forces to SWNTs via steric hindrance.

The efficacy of PI-BDA at dispersing SWNTs was quantitatively evaluated through absorption spectra measurement and Beer–Lambert law ($A = \epsilon lc$), where A is the absorbance at a particular wavelength (here we chose 500 nm), ϵ is the extinction coefficient, l is the path length (1 cm for our cell), and c is the concentration. To determine the extinction coefficient (ϵ), the absorbance of very dilute SWNT/PI-BDA (mass ratio 1:1) solution at different concentrations was measured. Figure 4A shows a representative curve and the absorbance at 500 nm plotted against SWNT concentrations (inset in Figure 4A). The linear-least-squares fit to the data gave a slope of 37.60, which was used to calculate the extinction coefficient (i.e., $\epsilon = 37.60 \text{ mL mg}^{-1} \text{ cm}^{-1}$) for determination of SWNT concentration. Figure 4B shows the extracted SWNT concentrations of SWNT/PI-BDA dispersions prepared using different PI-BDA to SWNT mass ratio from 0.125:1 to 2:1 in different conditions: (1) immediately after sonication; (2) after standing for 3 days, and (3) after centrifugation at 6000 rpm for 1 h. Immediately after sonication, all the

dispersions have suspended SWNT concentrations of about 0.02 mg/mL for ease of comparison among various PI-BDA to SWNT ratios. After standing for 3 days or centrifugation at 6000 rpm for 1 h, there is a clear dependence of the PI-BDA to SWNTs mass ratio on the amount of dispersed SWNTs. The SWNT concentration increases first but levels off when the PI-BDA to SWNTs mass ratio reaches 1:1, suggesting that 1:1 is the optimal mass ratio for preparing SWNT/PI-BDA dispersion. The SWNT concentration of SWNT/PI-BDA (mass ratio 1:1) after centrifugation is about 0.0158 mg/mL, which is higher than that of polyvinylpyrrolidone (PVP, $M_w = 29\,000$, Sigma-Aldrich) dispersed SWNTs prepared by the same method (0.0105 mg/mL), indicating higher efficacy of PI-BDA at dispersing SWNTs than the commercial dispersant PVP.³⁹

SWNT Dispersion and Interfacial Bonding in Composites.

Figure 5 shows the FE-SEM images of SWNTs in uncured SWNT(1 wt %)/R and SWNT(1 wt %)/PI-BDA/R spun fibers after removal of free polymer on a 0.2- μm Al_2O_3 membrane. Pristine SWNTs form large aggregates (Figure 5A1) while PI-BDA functionalized SWNTs are homogeneously dispersed (Figure 5B1). Higher magnification images reveal that SWNTs in SWNT/PI-BDA were debundled very well and the nanotube bundle size (Figure 5B2) is much smaller than that of pristine SWNTs (Figure 5A2). These observations are consistent with the dispersion state of pristine and PI-BDA functionalized SWNTs in the fully cured composite fibers that will be discussed below.

Figure 6 shows optical micrographs of fully cured SWNT/R and SWNT/PI-BDA/R composite fibers with SWNT loading of 0.2 wt %. (Composites with higher SWNT loadings are opaque.) Many black spots with sizes up to 10 μm can be clearly seen in the SWNT (0.2 wt %)/R fiber (Figure 6A), indicating nonuniform dispersion of SWNTs. In contrast, SWNT (0.2 wt %)/PI-BDA/R shows homogeneous dispersion of SWNTs throughout the matrix, and no obvious aggregates were observed (Figure 6B).

To further evaluate the dispersion and morphology of SWNTs in composite fibers, cross sections of SWNT-(1 wt %)/R and SWNT(1 wt %)/PI-BDA/R composite fibers after tensile testing were examined with FE-SEM (Figure 7). In SWNT(1 wt %)/R composite fibers, aggregates with sizes of about 1 μm can be clearly seen, indicating nonuniform dispersion (Figure 7A1, circled). Many SWNTs are pulled out, leaving holes on the surface (Figure 7A2 and A3, arrows), indicating weak interfacial adhesion between the SWNTs and the CE-EP matrix. In contrast, PI-BDA functionalized SWNTs are homogeneously distributed in the CE-EP matrix without any large aggregates (Figure 7B1). Some nanotubes seem to have partially pulled out from the surface but the pull-out length of the SWNTs is significantly reduced (indicated by squares in Figure 7B2 and B3) compared with the nanotubes in SWNTs/R; other nanotubes are broken on the surface and the ends

(37) Forrest, G. A.; Alexander, A. J. *J. Phys. Chem. C* **2007**, *111*, 10792.
(38) Yuen, S. M.; Ma, C. C. M.; Chiang, C. L.; Lin, Y. Y.; Teng, C. C. *J. Polym. Sci., Part A: Polym. Chem.* **2007**, *45*, 3349.

(39) Hasan, T.; Scardaci, V.; Tan, P. H.; Rozhin, A. G.; Milne, W. I.; Ferrari, A. C. *J. Phys. Chem. C* **2007**, *111*, 12594.

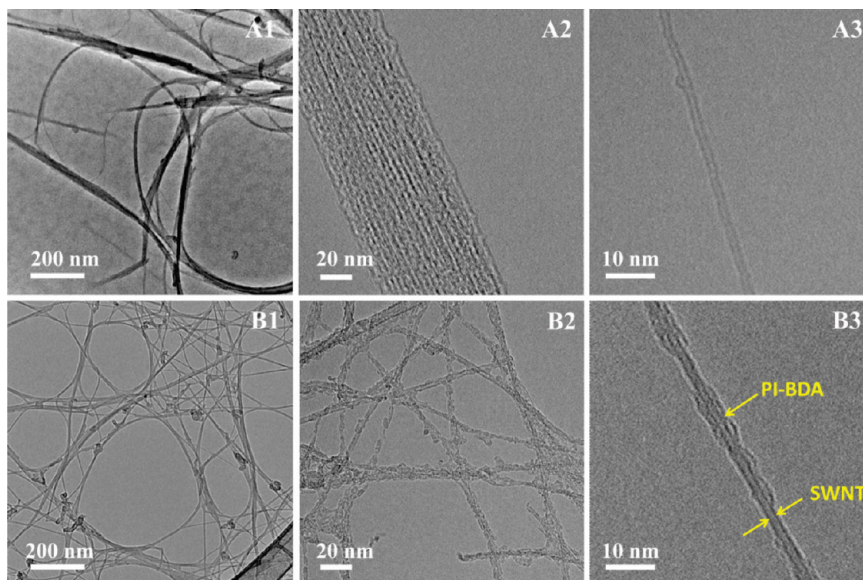


Figure 3. TEM images of (A1–A3) pristine SWNTs and (B1–B3) PI-BDA functionalized SWNTs.

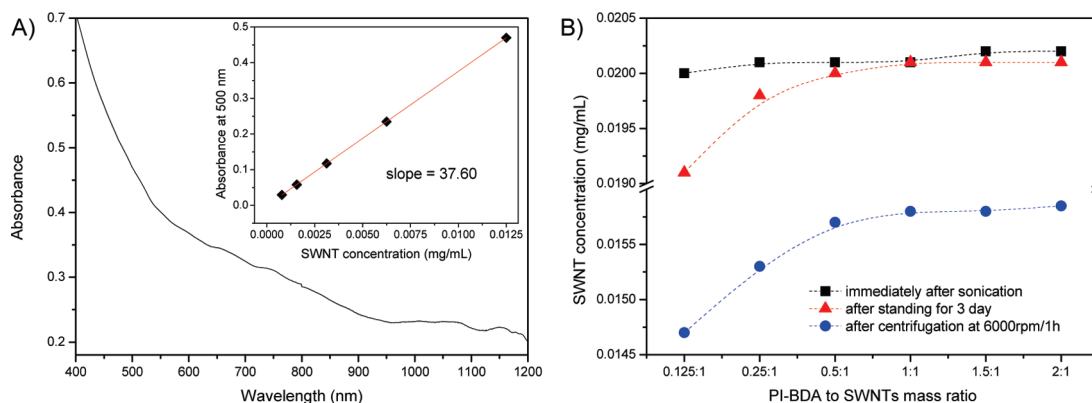


Figure 4. (A) Absorption spectrum of SWNTs/PI-BDA (mass ratio 1:1) at a concentration of 0.0125 mg/mL in DMF. Inset shows absorbance at 500 nm of the SWNTs/PI-BDA (1:1) in DMF at different concentrations. The straight line is a linear-least-squares fit to the data. (B) SWNT concentrations of solutions prepared using different PI-BDA to SWNT mass ratio in different conditions: immediately after sonication; after standing for 3 days, and after centrifugation at 6000 rpm for 1 h.

are tightly embedded in the matrix (indicated by circles in Figure 7B2 and B3). These FE-SEM images suggest that the nanotube/matrix interface between PI-BDA functionalized SWNTs and the CE-EP matrix is stronger than that in SWNT/R composite. The strong interfacial bonding can be ascribed to two effects: (i) strong π - π interaction between nanotube and the backbone of PI-BDA and (ii) the compatibility and covalent reaction between the BDA side chain and the matrix.

The π - π interaction between SWNTs and the backbone of PI-BDA was verified by Raman spectra. Figure 8A shows Raman spectra of (a) pristine SWNTs, (b) SWNTs/PI-BDA, (c) SWNT(1 wt %)/R fibers, and (d) SWNT-(1 wt %)/PI-BDA/R fibers. It is known that covalent functionalization can introduce defects into CNTs, leading to increased intensity of D-band (at about 1330 cm^{-1}).^{6,40} Unlike covalent functionalization, no significant increase

in the peak intensity of D-band was observed in SWNTs/PI-BDA (b) and SWNT(1 wt %)/PI-BDA/R (d), indicating that the nanotube graphene structure was well preserved after noncovalent functionalization with PI-BDA. Comparing the G band of SWNTs/PI-BDA (b), SWNTs(1 wt %)/R (c), and SWNTs(1 wt %)/PI-BDA/R (d) to the pristine SWNTs sample (a), upshifts of about 5, 3, and 7 cm^{-1} , respectively, were observed. The 3 cm^{-1} upshift in SWNTs(1 wt %)/R (c) compared to pristine SWNTs (a), and the 2 cm^{-1} higher upshift in SWNTs(1 wt %)/PI-BDA/R (d) compared to SWNTs/PI-BDA (b) can be attributed to the π -stacking of CE-EP resin molecules on the nanotubes.⁴¹ The 4 – 5 cm^{-1} Raman upshifts due to the PI-BDA (comparing d to c, and b to a) indicate that the electronic environment of the SWNT surface has changed after functionalization with PI-BDA, with or without CE-EP matrix. This is believed to be due to the strong π - π

(40) Peng, H. Q.; Alemany, L. B.; Margrave, J. L.; Khabashesku, V. N. *J. Am. Chem. Soc.* **2003**, *125*, 15174.

(41) Tournus, F.; Latil, S.; Heggge, M. I.; Charlier, J. C. *Phys. Rev. B* **2005**, *72*, 075431.

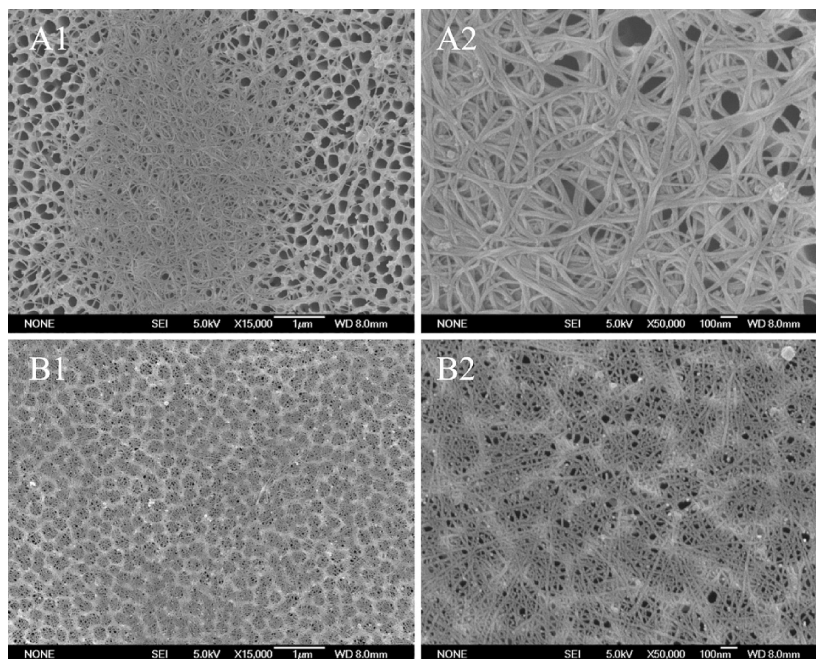


Figure 5. FE-SEM images of SWNTs in uncured (A1 and A2) SWNT(1 wt %)/R and (B1 and B2) SWNT(1 wt %)/PI-BDA/R spun fibers after removal of free polymer on a 0.2- μm Al_2O_3 membrane.

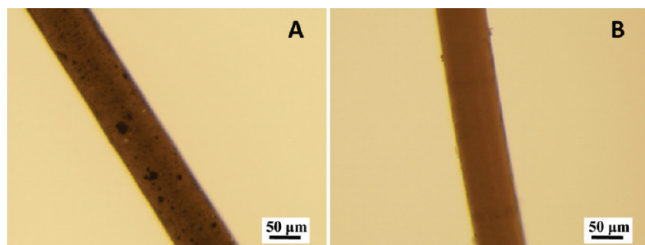


Figure 6. Optical micrographs of (A) SWNT (0.2 wt %)/R and (B) SWNT (0.2 wt %)/PI-BDA/R composite fibers after postcuring.

interaction between highly conjugated SWNT wall and PI-BDA backbone with high content of aromatic rings.^{23,25}

The BDA side chains also contribute to the good interfacial adhesion between SWNTs/PI-BDA and CE-EP matrix. The BDA side chain contains bisphenol A moiety like those in the cyanate ester and epoxy resins, which increases the compatibility and miscibility between SWNTs/PI-BDA and CE-EP matrix. Moreover, the $-\text{OH}$ groups on BDA side chains can react with $-\text{OCN}$ group of CE to form iminocarbonate ($-\text{OC}(\text{O}-)=\text{NH}$) bonds (Scheme 3).^{42–44} The formation of iminocarbonate was confirmed with FT-IR and ^1H NMR.

To increase detectability of the reaction between PI-BDA and CE, a blend containing larger proportions of PI-BDA to CE (30/70, w/w) was heated and analyzed with FT-IR and ^1H NMR. Figure 8B shows the FT-IR spectra of (a) neat CE before curing, (b) PI-BDA, and PI-BDA/CE (30/70, w/w) (c) before and (d) after heating at 120 $^\circ\text{C}$ for 1 h. In spectrum 8B(c), the band at 1678 cm^{-1} ,

attributed to the formation of new $-\text{OC}(\text{O}-)=\text{NH}$ bands,^{43,44} is present but small as the sample was heated to 80 $^\circ\text{C}$ (for DMF removal after casting). After further heating at 120 $^\circ\text{C}$ for 1 h (spectrum 8B(d)), the relative intensity of $-\text{OC}(\text{O}-)=\text{NH}$ band (1678 cm^{-1}) increased, suggesting the reaction of more $-\text{OH}$ groups with $-\text{OCN}$. The increased intensities of the bands at 1369 and 1567 cm^{-1} imply the formation of some triazine structures.³⁴ A control experiment was also performed in which pure CE without PI-BDA was used, and there was no difference in the FT-IR spectra of the pure CE treated at 80 $^\circ\text{C}/2$ h and 120 $^\circ\text{C}/1$ h (Data not shown).

The reaction between PI-BDA and CE was also confirmed by ^1H NMR spectra. Figure 8C shows the ^1H NMR spectra of PI-BDA/CE (30/70, w/w) mixture in $\text{DMSO}-d_6$ before and after heating at 120 $^\circ\text{C}$ for 1 h. After heating at 120 $^\circ\text{C}$ for 1 h (spectrum 8C(b)), the intensity of the peaks at around 9.2 ppm resulting from the NH protons of $-\text{OC}(\text{O}-)=\text{NH}$ groups⁴³ significantly increased. Additional evidence of reaction is that the $-\text{CH}_3$ peaks (at δ around 1.6 ppm) and aromatic peaks (at δ 6.7–7.2 ppm) of CE (overlapped with the peaks due to $-\text{CH}_3$ and aromatic protons in PI-BDA, respectively) split into two or more peaks, which can be attributed to unconsumed CE, and adducts between PI-BDA and CE (or triazine oligomer) (Scheme 3).⁴³ All these confirm that $-\text{OCN}$ groups on CE matrix covalently react with $-\text{OH}$ groups on PI-BDA dispersant to form $-\text{OC}(\text{O}-)=\text{NH}$ bonds.

Mechanical Properties. The tensile properties for neat CE-EP, SWNT/R, and SWNT/PI-BDA/R composites with different nanotube loadings are summarized in Table 1 and Figure 9. Representative tensile stress versus strain curves are shown in Figure 9A. Without adding PI-BDA dispersant, SWNTs/R composites show limited increases in tensile properties. The highest increase in tensile modulus

(42) Grigat, E.; Putter, R. *Angew. Chem., Int. Ed.* **1967**, *6*, 206.

(43) Lin, C. H. *Polymer* **2004**, *45*, 7911.

(44) Liang, K. W.; Li, G. Z.; Toghiani, H.; Koo, J. H.; Pittman, C. U. *Chem. Mater.* **2006**, *18*, 301.

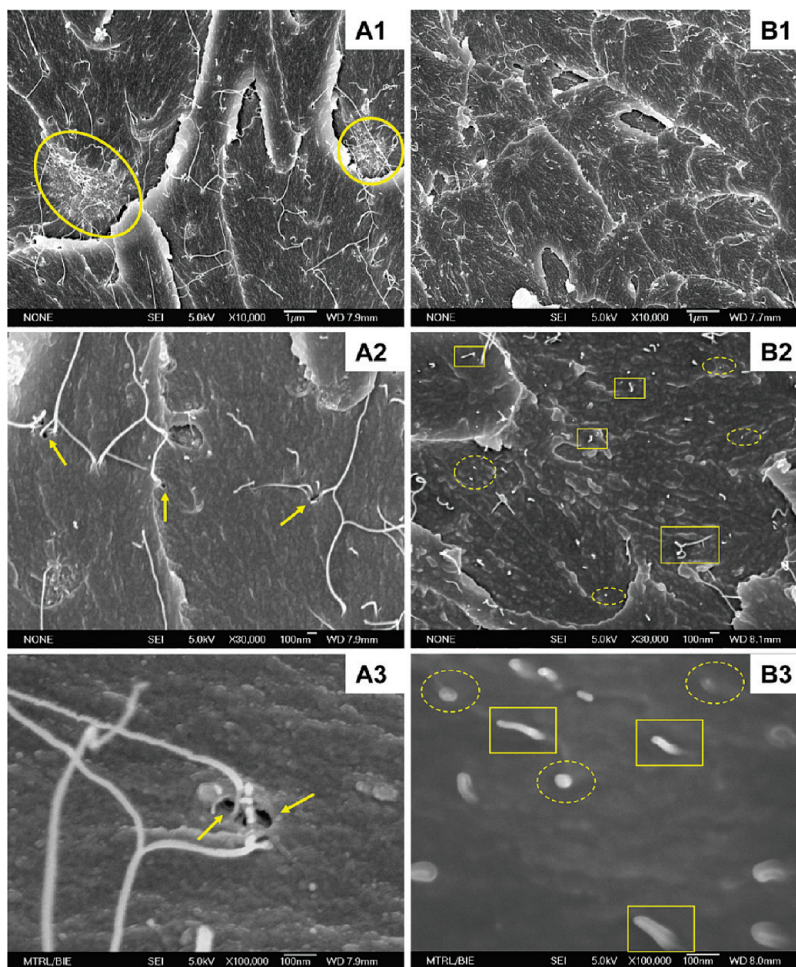


Figure 7. FE-SEM images of cross-sectional fracture surfaces of (A1–A3) SWNT(1 wt %)/R and (B1–B3) SWNT(1 wt %)/PI-BDA/R composites after tensile testing.

(E) is 33% (from 2.61 ± 0.14 to 3.47 ± 0.18 GPa) at SWNT loading of 1 wt %, and the highest increase in tensile strength (σ) is 28% (from 83.7 ± 3.3 to 107.0 ± 11.0 MPa) at SWNT loading of 0.5 wt %. Further increase in SWNT content impairs tensile properties. The elongation at break (ϵ) decreases continuously from 5.0 ± 0.4 to $2.5 \pm 0.4\%$ as SWNT loading increases from 0 to 1.5 wt %, and the toughness (T) has no significant improvement. With SWNTs dispersed by PI-BDA, increasing nanotube content from 0 to 1 wt % leads to a continuous increase in both tensile modulus and strength. For SWNT(1 wt %)/PI-BDA/R composite, the tensile modulus and strength increased by 80% and 70%, respectively, from 2.61 ± 0.14 to 4.70 ± 0.24 GPa and 83.7 ± 3.3 to 142.3 ± 6.9 MPa (relative to neat CE-EP resin). 1.5 wt % SWNTs/PI-BDA resulted in decreased tensile modulus and strength, which can be attributed to the poor wetting of SWNTs as reflected from more pulled-out SWNTs on the fracture surface of the SWNT(1.5 wt %)/PI-BDA/R composite (Supporting Information, Figure S7). Others have calculated that 1 vol % (~ 1 wt %) of SWNTs is sufficient to ensure that all of the polymer molecules are within one radius of gyration (5 nm) of a nanotube, implying difficulties in complete wetting of high loading (> 1 wt %)

of SWNTs.^{1,45} This theoretical estimate is consistent with our observation. The elongation at break of SWNT/PI-BDA/R composite increases initially at SWNT loading of 0.2 wt % (from 5.0 ± 0.4 to $6.2 \pm 0.7\%$) and then decreases gradually to $3.7 \pm 0.4\%$ for the 1.5 wt % composite. All the SWNT/PI-BDA/R composites with SWNT loading ranging from 0.2 to 1.5 wt % show higher toughness than neat CE-EP resin. Increases of 100% and 58% in toughness are achieved at SWNT loading of 0.2 wt % and 1 wt %, respectively. As manifested in the FE-SEM fractograph of the SWNT(1 wt %)/PI-BDA/R composite (Figure 7B1), well-dispersed SWNTs and strong SWNT-matrix bonding effectively resist the propagation of cracks during deformation,³⁴ thus increasing the fracture toughness. The poor reinforcement effect of SWNTs without dispersant is possibly due to the aggregation of nanotubes in the matrix and weak interfacial bonding as discussed previously. This is corroborated by greater improvements of the tensile modulus, strength, and toughness of the composites with the PI-BDA dispersant.

Using only 1 wt % PI-BDA functionalized SWNTs, the absolute tensile properties of SWNT(1 wt %)/PI-BDA/R composites ($E = 4.70 \pm 0.24$ GPa and $\sigma = 142.3 \pm 6.9$ MPa) are higher than those of most other CNT reinforced thermoplastics and thermosets, including CNT/CE¹⁰ and

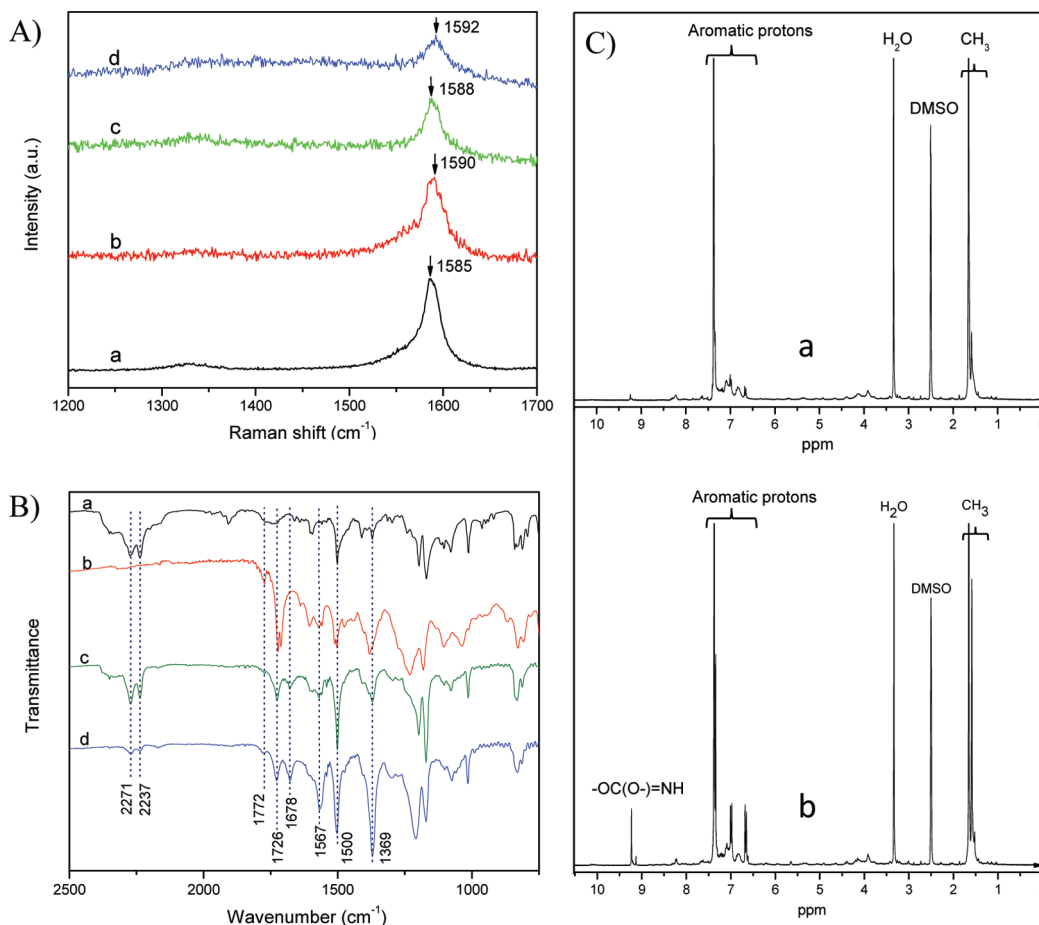


Figure 8. (A) Raman spectra of (a) pristine SWNTs, (b) SWNTs/PI-BDA, (c) SWNT(1 wt %)/R composites, and (d) SWNT(1 wt %)/PI-BDA/R composites. (B) FT-IR spectra of (a) neat CE before curing, (b) PI-BDA, (c) and (d) PI-BDA/CE (30/70, w/w) (c) before and (d) after heating at 120 °C for 1 h. (C) ^1H NMR spectra of PI-BDA/CE (30/70, w/w) in $\text{DMSO}-d_6$ (a) before and (b) after heating 120 °C for 1 h.

CNT/epoxy^{6,7,11,46–48} thermosetting composites. Because no work appears about CNTs reinforced CE-EP composite, here we compare our results with that of solution-processed CNTs reinforced epoxy (a typical thermosetting matrix) composites. The detailed comparison is summarized in Table S1 in Supporting Information. It should be noted that the comparisons are only approximate as the nanotubes used, matrices, processing technique (e.g., solution mixing versus direct mixing), etc., which are listed in Table S1 differ. Nanotubes used could be single-walled, double-walled, or multiwalled.^{6,8,48} From Table S1, we can see that most tensile properties are reported for low CNT contents (about 1 wt %) as the mechanical properties usually deteriorate with higher loadings. While the epoxy resins used differ chemically, most have strength (σ) and modulus (E) of about 60–90 MPa and 2–3 GPa, respectively. The reported nanotube dispersion methods for the tabulated composites involve covalent functionalizations.^{6,11} Our absolute values and percent increases

for both tensile strength and modulus achieved with 1 wt % of SWNTs/PI-BDA ($E = 4.70 \pm 0.24$ GPa (80% increase) and $\sigma = 142.3 \pm 6.9$ MPa (70% increase)) are higher than the tabulated increases for E and σ which are usually less than 30–40%^{7,11,47} The tensile reinforcement efficacy can also be quantitatively evaluated by calculating the Young's modulus and tensile strength per unit weight fraction (dE/dW_{NT} and $d\sigma/dW_{\text{NT}}$).^{11,49} In this study, dE/dW_{NT} and $d\sigma/dW_{\text{NT}}$ reach to 252 GPa and 8120 MPa, respectively, at 0.5 wt % of SWNTs and to 209 GPa and 5860 MPa at 1 wt % of SWNTs. These values are also superior compared to the results of CNT/epoxy composites reported recently (Supporting Information, Table S1).^{6,7,11,47,48} The significant mechanical enhancements achieved here can be attributed to the (i) high aspect ratio of SWNTs with well-preserved graphene structure surface due to noncovalent functionalization; (ii) homogeneous dispersion of SWNTs/PI-BDA in CE-EP matrix; and (iii) strong π - π interaction between SWNTs and the backbone of PI-BDA, and covalent reaction between PI-BDA dispersant and the CE-EP matrix.

The tensile strength of CE-EP composites reinforced with SWNTs can be predicted by a standard model for

(46) Spitalsky, Z.; Tasis, D.; Papagelis, K.; Galiotis, C. *Prog. Polym. Sci.* **2010**, *35*, 357.

(47) Zhu, J.; Peng, H. Q.; Rodriguez-Macias, F.; Margrave, J. L.; Khabashesku, V. N.; Imam, A. M.; Lozano, K.; Barrera, E. V. *Adv. Funct. Mater.* **2004**, *14*, 643.

(48) Gojny, F. H.; Wichmann, M. H. G.; Fiedler, B.; Schulte, K. *Compos. Sci. Technol.* **2005**, *65*, 2300.

(49) Yan, Y. H.; Zhao, S. A.; Cui, J.; Yang, S. B. *J. Polym. Sci., Part A: Polym. Chem.* **2009**, *47*, 6135.

Scheme 3. Schematic of Reactions between –OH Groups on PI-BDA and CE (or its Oligomer)

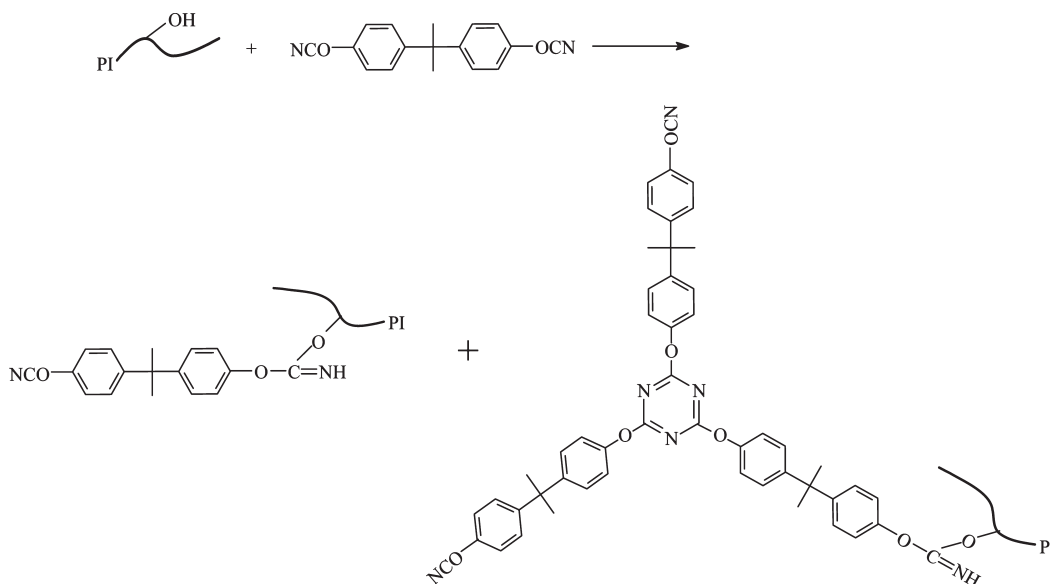


Table 1. Mechanical and Thermal Properties of Neat CE-EP and its Nanocomposites

sample	E (GPa)	σ (MPa)	ϵ (%)	T^a (MJ m ⁻³)	T_g^b (°C)	T_d^c (°C)
neat CE-EP	2.61 ± 0.14	83.7 ± 3.3	5.0 ± 0.4	2.6 ± 0.2	167	305
SWNTs (0.2 wt %)/R	3.37 ± 0.07	103.1 ± 8.5	4.7 ± 0.7	3.0 ± 0.4	167	307
SWNTs (0.5 wt %)/R	3.38 ± 0.10	107.0 ± 11.0	4.7 ± 0.6	2.9 ± 0.2	165	311
SWNTs (1 wt %)/R	3.47 ± 0.18	100.1 ± 6.5	3.9 ± 0.4	2.5 ± 0.3	162	317
SWNTs (1.5 wt %)/R	3.10 ± 0.19	70.6 ± 4.6	2.5 ± 0.4	1.0 ± 0.2	159	318
SWNTs (0.2 wt %)/PI-BDA/R	3.48 ± 0.15	120.1 ± 2.7	6.2 ± 0.7	5.2 ± 0.6	175	308
SWNTs (0.5 wt %)/PI-BDA/R	3.87 ± 0.09	124.3 ± 2.2	4.8 ± 0.4	4.2 ± 0.3	170	317
SWNTs (1 wt %)/PI-BDA/R	4.70 ± 0.24	142.3 ± 6.9	4.2 ± 0.8	4.1 ± 0.4	164	323
SWNTs (1.5 wt %)/PI-BDA/R	4.40 ± 0.34	124.8 ± 9.6	3.7 ± 0.4	2.9 ± 0.3	160	320

^a Calculated from the area under the stress–strain curve. ^b The glass transition temperature determined by differential scanning calorimetry. ^c Thermal decomposition at 5 wt % weight loss.

composite reinforced with short aligned fibers:^{10,50}

$$\sigma_C = \left(1 - \frac{\sigma_f r}{2l_f \tau}\right) \sigma_f V_f + \sigma_m (1 - V_f)$$

where σ_C , σ_f , and σ_m are the composite, the nanotube, and the polymer matrix strengths, respectively; r is average SWNT radius; l_f is average SWNT length; V_f is the SWNT volume fraction (estimated from the SWNT mass fraction, the SWNT density (1.5 g cm⁻³), and the matrix density (1.2 g cm⁻³)); and τ is the nanotube–matrix interfacial shear strength. Based on the values $\sigma_f = 30$ GPa,² $\sigma_m = 83.7$ MPa, $r = 5$ nm, $l_f = 5$ μ m, and $\tau = 150$ MPa,⁵¹ the theoretical tensile strengths of composites with SWNTs loading of 0.2, 0.5, 1.0, and 1.5 wt % are 129, 197, 311, and 425 MPa, respectively. By comparing with the respective measured strength values of 120.1 ± 2.7, 124.3 ± 2.2, 142.3 ± 6.9, and 124.8 ± 9.6 MPa, we see that our measured strength is very close to the calculated value

only for SWNT(0.2 wt %)/PI-BDA/R. The measured strength values diverge from the calculated data as the SWNT loading increases beyond 0.2 wt %. The possible reason may include limited alignment of SWNTs in the composite fiber, relatively weak interaction between SWNTs and PI-BDA, inevitable SWNT bundling, fiber defect, and so on. We also believe that the adhesion of the matrix to the nanotube at high nanotube loading is relatively poor with this dispersant since the interaction is noncovalent. These negative influences become severe at high SWNT loadings.

To make better improvements in the mechanical properties with nanotube, especially at high loading of the latter, several criteria need to be simultaneously achieved: good nanotube wetting and dispersion, low nanotube defect, nanotube alignment, and good stress transfer to the matrix. It appears that for multiwalled carbon nanotubes with diameters of about 10 nm, the theoretical limit of nanotube content for good wetting is around 30 wt %.¹ Ensuring good stress transfer to the atomically smooth nanotube surface may be another major challenge that needs to be overcome. Also, it will be ideal to have a matrix that is also nanotube-dispersing without involving

(50) Hull, D. *Cambridge Solid State Science Series: An Introduction to Composite Materials*; Cambridge University Press: Cambridge, 1988.
 (51) Barber, A. H.; Cohen, S. R.; Eitan, A.; Schadler, L. S.; Wagner, H. D. *Adv. Mater.* **2006**, *18*, 83.

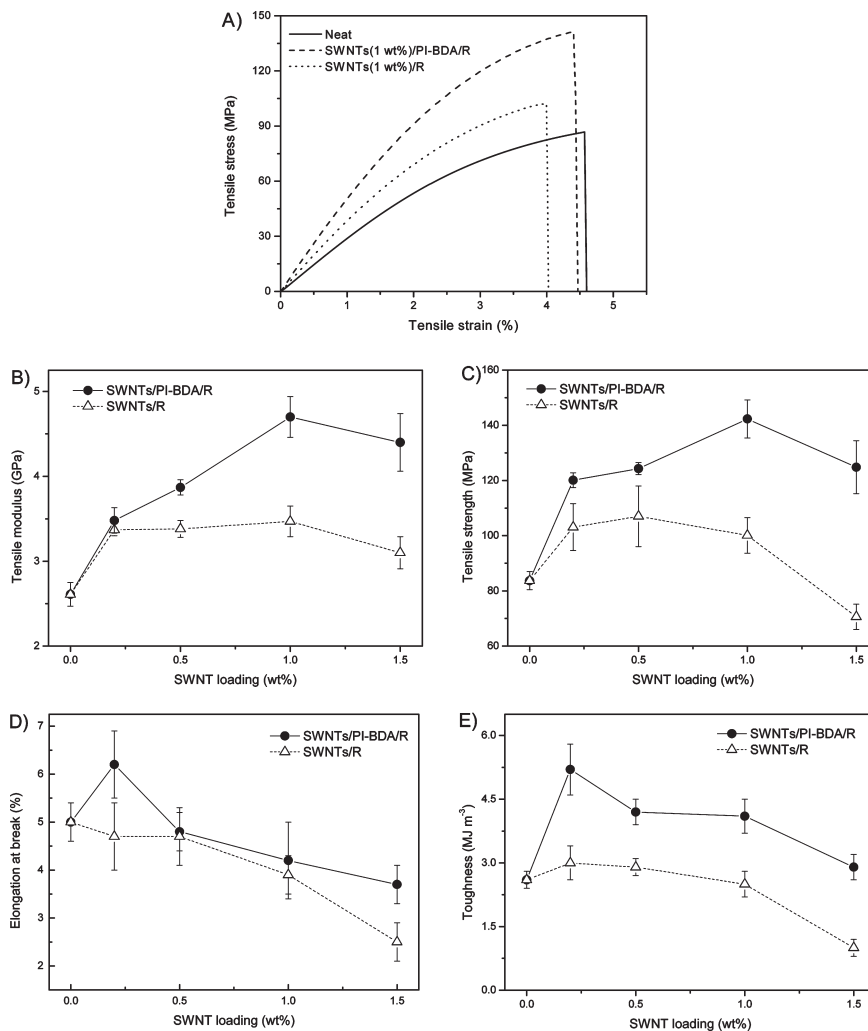


Figure 9. (A) Representative stress–strain curves of neat CE-EP, SWNT(1 wt %)/R, and SWNT(1 wt %)/PI-BDA/R composites. (B) Tensile modulus, (C) tensile strength, (D) elongation at break, and (E) toughness of SWNT/PI-BDA/R and SWNT/R composites with different SWNT loadings.

a dispersant or surfactant that is different from the matrix as the compatibility of the matrix and dispersant/surfactant is usually poor. We are exploring some of these factors in trying to improve the properties of nanotube-reinforced composites.

Thermal Properties. With addition of the PI-BDA dispersant, the thermal properties (specifically glass transition temperature (T_g) and decomposition temperature (T_d)) of the SWNT/PI-BDA/R composites were improved compared with SWNT/R composites or neat resin (Table 1). Good nanotube dispersion and interfacial reaction between CE matrix and SWNT/PI-BDA restricts the segmental motion of CE-EP molecules, leading to increased T_g .^{52,53} The reduction in T_g with further increase in CNT content may be possibly due to SWNT disruption of the cross-linking network of the matrix to reduce the effective cross-link density.⁵⁴ The improved thermal stability with addition of nanotubes is postulated to be due to a

nanotube barrier effect which retards the volatilization of polymer decomposition products, and the higher heat capacity of CNTs compared to polymer matrix.

Conclusions

We have designed and successfully synthesized PI-BDA, a reactive comb-like polymer, and have shown it to be highly effective in individually dispersing SWNTs and improving the mechanical and thermal properties of the SWNT-reinforced CE-EP composite fibers. Only 1 wt % of PI-BDA functionalized SWNTs increased the tensile modulus, strength, and toughness of composite by 80% (to 4.70 ± 0.24 GPa), 70% (to 142.3 ± 6.9 MPa), and 58% (to 4.1 ± 0.4 MJ m⁻³) over that of neat resin blend (with $E = 2.61 \pm 0.14$ GPa, $\sigma = 83.7 \pm 3.3$ MPa, and $T = 2.6 \pm 0.2$ MJ m⁻³). Without PI-BDA dispersant, the corresponding changes in mechanical properties when reinforced with 1 wt % SWNTs were 33%, 28%, and -4%. The polyimide backbone has strong π - π interaction with nanotubes to anchor the PI-BDA dispersant to them while the reactive BDA side chain provides steric stabilization and reacts with the CE resin during the thermal

(52) Tseng, C. H.; Wang, C. C.; Chen, C. Y. *Chem. Mater.* **2007**, *19*, 308.

(53) An, L.; Pan, Y. Z.; Shen, X. W.; Lu, H. B.; Yang, Y. L. *J. Mater. Chem.* **2008**, *18*, 4928.

(54) Putz, K. W.; Palmeri, M. J.; Cohn, R. B.; Andrews, R.; Brinson, L. C. *Macromolecules* **2008**, *41*, 6752.

cure. Our novel dispersant covalently reacts with the CE matrix through the side chain but strongly noncovalently interacts with nanotube surface to produce good nanotube dispersion with minimal damage to the CNTs, resulting in hence excellent reinforcement.

Acknowledgment. We gratefully acknowledge the financial support from the Defense & Science Technology Agency of Singapore (POD0513240) and Singapore National Research

Foundation through a Competitive Research Program grant (NRFCRP2-2007-02).

Supporting Information Available: Details of fiber fabrication, low-magnification TEM image of PI-BDA functionalized SWNTs, UV-vis-NIR spectroscopy, FE-SEM image of fracture surface of SWNT (1.5 wt %)/PI-BDA/R composite, and detailed comparison of our tensile properties with reported data of CNT/epoxy composites. This material is available free of charge via the Internet at <http://pubs.acs.org>.